

Dynamical properties of ultracold bosons in an optical lattice

S.D. Huber¹, E. Altman², H.P. Büchler^{3,4}, and G. Blatter¹

¹*Theoretische Physik, ETH Zurich, CH-8093 Zurich, Switzerland*

²*Department of Condensed Matter Physics, The Weizmann Institute of Science Rehovot, 76100, Israel*

³*Institute for Quantum Optics and Quantum Information of the Austrian Academy of Science, 6020 Innsbruck, Austria and*

⁴*Institut für theoretische Physik, Universität Innsbruck, 6020 Innsbruck, Austria*

(Dated: March 23, 2022)

We study the excitation spectrum of strongly correlated lattice bosons for the Mott-insulating phase and for the superfluid phase close to localization. Within a Schwinger-boson mean-field approach we find two gapped modes in the Mott insulator and the combination of a sound mode (Goldstone) and a gapped (Higgs) mode in the superfluid. To make our findings comparable with experimental results, we calculate the dynamic structure factor as well as the linear response to the optical lattice modulation introduced by Stöferle *et al.* [Phys. Rev. Lett. **92**, 130403 (2004)]. We find that the puzzling finite frequency absorption observed in the superfluid phase could be explained via the excitation of the gapped (Higgs) mode. We check the consistency of our results with an adapted f -sum-rule and propose an extension of the experimental technique by Stöferle *et al.* to further verify our findings.

PACS numbers: 03.75.Kk, 39.25.+k

I. INTRODUCTION

The prime example of a strongly correlated Bose system is ⁴He — it exhibits normal, superfluid, crystalline, and possibly even supersolid phases^{1,2,3} and is attracting interest to this day.⁴ Dilute cold bosonic atoms reside generically in the weakly interacting limit but their tunability through quantum optical techniques allows for the realization of strongly correlated states. One way to achieve the strongly interacting limit is to reduce the kinetic energy by the application of an optical lattice, thereby effectively enhancing the effects of interactions. The broken translational symmetry then leads to new effects in the superfluid phase not present in ⁴He. The present paper is devoted to a study of the dynamical properties of lattice bosons within this strongly correlated regime.

Jaksch *et al.*⁵ pointed out that bosons in optical lattices are accurately described by the Bose-Hubbard Hamiltonian.⁶ Depending on the value of the nearest-neighbor hopping amplitude J , the on-site interaction U , and the chemical potential μ , the Bose-Hubbard model exhibits a superfluid or an insulating (with $n_0 \in \mathbb{N}$ particles per site) ground state, separated by a quantum phase transition.⁷ The phase diagram has been investigated on a mean-field level,^{6,8} using perturbation theory⁹ and with numerical quantum Monte Carlo methods.^{10,11} Apart from one dimension, the qualitative structure of the phase diagram is correctly described by mean-field calculations, cf. Fig. 1; however, fluctuations tend to shift the lobes to lower values of J/U in two dimensions.¹¹

The dynamical properties of the Bose-Hubbard model were studied in both the Mott and the superfluid phase. In the Mott phase, the excitation spectrum was studied numerically,^{9,12,13} on a mean-field level,⁸ in a slave-particle approach,^{14,15} and in strong coupling perturbation theory.

^{16,17} All these approaches yield two gapped modes describing hole- and particle-type branches. For the weakly interacting superfluid ($J \gg U$) the Gross-Pitaevskii^{18,19} equation and Bogoliubov theory²⁰ produce reliable results for the sound mode. However, for the superfluid close to localization the character of the spectrum is still unclear. We will show below that this spectrum involves two distinct modes: (i) a sound mode

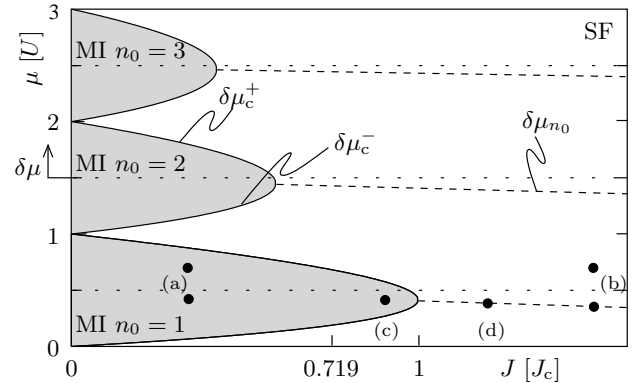


FIG. 1: The mean-field phase diagram of the Bose-Hubbard model involves disconnected incompressible Mott-insulating phases (grey shaded areas at small hopping J) where the density is pinned at integer values n_0 , and a connected superfluid phase in between and at larger values of J . The lines $\delta\mu_c^\pm$ mark the second order quantum phase transition separating these phases. The commensurate filling in the Mott lobes is exported into the superfluid along the lines $\delta\mu_{n_0}$ (bent downward) where particle-hole symmetry is preserved. In our analysis we use a truncation scheme allowing us to discuss one lobe at a time. The black dots mark the positions in phase space where the spectra of Fig. 2 have been evaluated. The chemical potential difference $\delta\mu$ is measured away from the lobe midpoint at $J = 0$.

characterized by a combined phase and density modulation, and (ii) a gapped mode describing exchange between condensate and noncondensate at fixed overall density.

The excitations of strongly correlated lattice bosons have been probed in two experiments. In the experiment by Greiner *et al.*⁷ the whole lattice has been subjected to a global tilt. As this perturbation spoils the translation invariance, it is difficult to infer bulk properties from their results; the observed resonant response has been discussed in Ref. 21. Second, in their recent experiment, Stöferle *et al.*,²² determine the energy absorption due to a modulation of the lattice depth. They find a gapped continuum of excitations for small J/U and a broad feature in the superfluid. The appropriate response function has been calculated in the framework of the Gross-Pitaevskii equation²³ and for one-dimensional systems (1D), both numerically^{13,24} and analytically.^{25,26} A more powerful method to investigate this system is Bragg spectroscopy,²⁷ described by the dynamic structure factor $S(\mathbf{q}, \omega)$. As compared to the above lattice modulation technique, Bragg spectroscopy allows for a nonzero momentum transfer and hence reveals the full structure of the excitation spectrum. However, the nonzero momentum transfer requires to apply two additional lasers at a finite angle to the system; so far, the limited optical access has hindered an experiment using Bragg spectroscopy on strongly correlated lattice bosons. On the theory side, the structure factor $S(\mathbf{q}, \omega)$ has been calculated in mean-field theory²⁸ and for 1D systems using numerical methods.^{29,30} Below, we calculate both response functions within the Mott insulator as well as in the strongly correlated superfluid, making use of one unified description.

Our method is based on a technique previously introduced by Altman and Auerbach³¹ describing the particle-hole symmetric limit of the Bose-Hubbard model at large particle numbers $n_0 \gg 1$. Here, we generalize this approach to deal with the experimentally relevant regime of Mott insulators with one and two particles per lattice site. The method involves a truncation of the Hilbert space to three states per site and a spin-wave technique within a slave-boson language to describe fluctuations above a mean-field ground state. The truncation limits the validity of our results to a single Mott lobe and its surrounding superfluid environment.

In the following Sec. II, we introduce the variational mean-field method outlined above. After proper truncation of the Hilbert space, we construct the mean-field phase diagram using a variational ground state. We proceed with the derivation of an effective Hamiltonian describing residual particle fluctuations using a method motivated by the mapping to a spin-1 Hamiltonian. We diagonalize this effective Hamiltonian with the help of a generalized Bogoliubov transformation and find the spectra in both insulating and superfluid phases. Section III is devoted to the study of the response functions: we discuss the dynamic structure factor (density-density corre-

lations) in the Mott phase as well as in the superfluid and compare our findings with previously obtained theoretical results. In addition to Bragg spectroscopy, we analyze the lattice modulation technique which is described in terms of a dynamic modulation of the tunneling amplitude J and calculate the corresponding response function (hopping correlator) in both phases and for varying dimensionality of the excitation. We summarize and conclude our work in Sec. IV.

II. VARIATIONAL MEAN-FIELD

A. Method

The Bose-Hubbard Hamiltonian in a notation suitable for our approximation scheme takes the form

$$H_{\text{BH}} = -J \sum_{\langle i,j \rangle} a_i^\dagger a_j + \frac{U}{2} \sum_i \delta n_i^2 - \delta\mu \sum_i n_i, \quad (1)$$

where a_i^\dagger is the bosonic creation operator for a Wannier state at site i , $n_i = a_i^\dagger a_i$ is the number operator and $\delta n_i = n_i - n_0$ measures deviations of the particle number from a mean filling n_0 . The chemical potential $\delta\mu$ is measured from the middle of the lobe (cf. Fig. 1).

Our goal is the determination of the dynamical properties of the Bose-Hubbard model in the limit of strong interactions. In particular, we are interested in finding the excitation spectra and eigenstates in the Mott-insulating as well as in the superfluid phase nearby. Note that weakly interacting theories such as the Gross-Pitaevskii equation or the Bogoliubov theory cannot capture the physics close to localization. On the other hand, strong coupling perturbative approaches are often incapable to correctly describe the broken U(1)-symmetry phase.¹⁶ Altman and Auerbach³¹ introduced a Hilbert space truncation method for large filling $n_0 \gg 1$, i.e., the particle-hole symmetric case, which we extend to low fillings where particle-hole symmetry is broken. The basic idea is to truncate the bosonic Fock space to only three local states. In this truncated space, we first find a variational (mean-field) ground state and then derive an effective Hamiltonian H_{eff} for the excitations above this ground state.

The truncation to three local states with particle numbers n_0 and $n_0 \pm 1$ is motivated by the strong suppression of particle number fluctuations in, and close to, the Mott phase; its validity is discussed in Sec. II C, below. We introduce bosonic operators that create ‘particles’ in the

retained three states

$$\begin{aligned} t_{1,i}^\dagger |\text{vac}\rangle &= \frac{(a_i^\dagger)^{n_0+1}}{\sqrt{(n_0+1)!}} |\text{vac}\rangle, \\ t_{0,i}^\dagger |\text{vac}\rangle &= \frac{(a_i^\dagger)^{n_0}}{\sqrt{n_0!}} |\text{vac}\rangle, \\ t_{-1,i}^\dagger |\text{vac}\rangle &= \frac{(a_i^\dagger)^{n_0-1}}{\sqrt{(n_0-1)!}} |\text{vac}\rangle, \end{aligned} \quad (2)$$

where $|\text{vac}\rangle$ denotes the state with no particles present. The original bosonic operators a_i can be expressed in terms of the $t_{\alpha,i}$ -operators ($\alpha = -1, 0, 1$),

$$a_i^\dagger = \sqrt{n_0+1} t_{1,i}^\dagger + \sqrt{n_0} t_{0,i}^\dagger + \sqrt{n_0-1} t_{-1,i}^\dagger. \quad (3)$$

The Hilbert space spanned by the $t_{\alpha,i}$ -operators is too large and the physical subspace is obtained by imposing the constraint

$$\sum_{\alpha=-1}^1 t_{\alpha,i}^\dagger t_{\alpha,i} = \mathbb{1}. \quad (4)$$

The possibility to map the above truncated bosonic problem to a spin-1 Hamiltonian (see Appendix A) motivates a strategy inspired by the spin-wave theory above a ferromagnetic or antiferromagnetic ground state:³² starting out by expressing the spin operators S_\pm and S_z via Schwinger bosons $a_{\text{SB}}^\dagger, b_{\text{SB}}^\dagger$: $S_+ = a_{\text{SB}}^\dagger b_{\text{SB}}$, $S_- = b_{\text{SB}}^\dagger a_{\text{SB}}$, and $S_z = (a_{\text{SB}}^\dagger a_{\text{SB}} - b_{\text{SB}}^\dagger b_{\text{SB}})/2$, the constraint $a_{\text{SB}}^\dagger a_{\text{SB}} + b_{\text{SB}}^\dagger b_{\text{SB}} = 2S$ is used in the ordered phase to go over to Holstein-Primakoff bosons $b_{\text{SB}}^\dagger \rightarrow b_{\text{HP}}^\dagger$ and $a_{\text{SB}}^\dagger \rightarrow \sqrt{2S} - b_{\text{HP}}^\dagger b_{\text{HP}}$, with subsequent expansion of the square root in $b_{\text{HP}}^\dagger b_{\text{HP}}$. In order to realize this program in the present situation, we first have to find the ground state playing the role of the ordered state in the spin problem. In a second step, we implement the holonomic constraint (4) via a procedure analogous to the change from Schwinger to Holstein-Primakoff bosons.

In order to find a proper ground state of the truncated problem we introduce the following variational operators

$$\begin{aligned} b_{0,i}^\dagger &= \cos(\vartheta/2) t_{0,i}^\dagger + \sin(\vartheta/2) [\cos(\chi) t_{1,i}^\dagger + \sin(\chi) t_{-1,i}^\dagger], \\ b_{1,i}^\dagger &= -\sin(\vartheta/2) t_{0,i}^\dagger + \cos(\vartheta/2) [\cos(\chi) t_{1,i}^\dagger + \sin(\chi) t_{-1,i}^\dagger], \\ b_{2,i}^\dagger &= -\sin(\chi) t_{1,i}^\dagger + \cos(\chi) t_{-1,i}^\dagger, \end{aligned} \quad (5)$$

where the Gutzwiller-type ground state shall be given by

$$|\Psi(\vartheta, \chi)\rangle = \prod_i b_{0,i}^\dagger |\text{vac}\rangle. \quad (6)$$

The parameter ϑ controls the admixture of particle number fluctuations in the ground state, whereas a deviation from integer filling is accounted for by a nonvanishing $\sigma = \pi/4 - \chi$. As the transformation (5) is unitary, the $b_{m,i}$ operators ($m = 0, 1, 2$) obey the constraint

$$\sum_{m=0}^2 b_{m,i}^\dagger b_{m,i} = \mathbb{1}, \quad (7)$$

cf. (4). The relevant energy scale in the Mott phase is given by the interaction strength U . For the discussion of the phase diagram all energies are rescaled and denoted with a bar, e.g., $\bar{J} = J/U$. Combining the Hamiltonian (1) and the ansatz (6) provides us with the variational energy per lattice site $\bar{\varepsilon}_{\text{var}}(\vartheta, \sigma) = \langle \Psi(\vartheta, \sigma) | \bar{H}_{\text{BH}} | \Psi(\vartheta, \sigma) \rangle / N$ which is given by

$$\begin{aligned} \bar{\varepsilon}_{\text{var}}(\vartheta, \sigma) &= \sin(\vartheta/2)^2 \left[\frac{1}{2} - \delta\bar{\mu} \sin(2\sigma) \right] - \frac{\bar{J}z}{4} \sin^2(\vartheta) \\ &\times \left[n_0 + \sqrt{(n_0+1)n_0} \cos(2\sigma) + \frac{1}{2}(1 + \sin(2\sigma)) \right], \end{aligned} \quad (8)$$

where $z = 2d$ is the coordination number and N denotes the number of sites. In the Mott-insulating phase, particle number fluctuations are absent within a mean-field approximation and thus $\vartheta = 0$; the parameter σ then drops out of the variational energy $\bar{\varepsilon}_{\text{var}}(\vartheta, \sigma)$ and can be set to zero. In the superfluid case, $\vartheta \neq 0$ turns out to be a convenient order parameter and hence σ is eliminated via minimization of the variational energy (8) with respect to σ ,

$$\sigma(\vartheta) = \frac{1}{2} \arctan \left(\frac{4\delta\bar{\mu} + \bar{J}z[\cos(\vartheta) + 1]}{2\bar{J}z[\cos(\vartheta) + 1]\sqrt{n(n+1)}} \right). \quad (9)$$

This allows us to write $\bar{\varepsilon}_{\text{var}}(\vartheta, \sigma)$ as a function of ϑ alone. Within a Ginzburg-Landau treatment of the phase transition, we reexpress ϑ in terms of the superfluid order parameter parameter $\psi = \langle \Psi(\vartheta, \sigma) | a_i | \Psi(\vartheta, \sigma) \rangle / N = \sin(\vartheta)[\sqrt{n_0+1} \cos(\pi/4-\sigma) + \sqrt{n_0} \sin(\pi/4-\sigma)]/2$ and expand the variational energy (8) in ψ ,

$$\bar{\varepsilon}_{\text{var}}(\vartheta, \sigma(\vartheta)) \approx \bar{a}(\bar{J}, \delta\bar{\mu}) \psi^2 + \frac{\bar{b}(\bar{J}, \delta\bar{\mu})}{2} \psi^4. \quad (10)$$

The calculation of the coefficients $\bar{a}(\bar{J}, \delta\bar{\mu})$ and $\bar{b}(\bar{J}, \delta\bar{\mu})$ is straightforward. The sign change of $\bar{a}(\bar{J}, \delta\bar{\mu})$ marks the phase boundary and the roots of $\bar{a}(\bar{J}, \delta\bar{\mu}) = 0$ provide us with the known mean-field lobes

$$\delta\bar{\mu}_c^\pm(\bar{J}) = \frac{1}{2} \left[-\bar{J}z \pm \sqrt{1 - 2\bar{J}z(1+2n_0) + (\bar{J}z)^2} \right], \quad (11)$$

cf. Fig. 1. The tip of the lobes can be found by equating $\delta\bar{\mu}_c^+ = \delta\bar{\mu}_c^-$, providing the critical hopping $z\bar{J}_c = 1/(\sqrt{n_0+1} + \sqrt{n_0})^2$. Due to particle-hole asymmetry, the line of integer density ($\sigma = 0$) is bending down according to (cf. Fig. 1)

$$\delta\bar{\mu}_{n_0} = -\frac{1}{4} [\bar{J}z + (\sqrt{n_0+1} + \sqrt{n_0})^{-2}]; \quad (12)$$

we refer to this line as the particle-hole symmetric line, which starts out from the tip of the lobe $\delta\bar{\mu}_c^\pm(\bar{J}_c)$ as expected.

The above determination of the ground state (6) has provided us with the phase diagram of the Bose Hubbard model and allows us to proceed with the second step of

our program, the implementation of the constraint (7) by going over to Holstein-Primakoff-type bosons; thereby, the operator $b_{0,i}^\dagger$ plays the role of the Schwinger boson a_{SB}^\dagger and the remaining operators $b_{1,i}^\dagger$, $b_{2,i}^\dagger$ generate the excitations above this ground state, as does the operator b_{HP}^\dagger in the spin problem. We then eliminate one slave boson ($b_{0,i}$) via the constraint

$$b_{0,i} = \sqrt{1 - n_{1,i} - n_{2,i}}, \quad (13)$$

where $n_{m,i} = b_{m,i}^\dagger b_{m,i}$ ($m = 1, 2$). Having chosen a good ‘classical’ ground state with potentially small fluctuations, we can expand the square root in (13)

$$b_{0,i} = \sqrt{1 - n_{1,i} - n_{2,i}} \approx (1 - \tfrac{1}{2}n_{1,i} - \tfrac{1}{2}n_{2,i}); \quad (14)$$

the validity of the expansion will be discussed later (cf. Sec. II C).

We express the Hamiltonian (1) in terms of the b bosons and eliminate the $b_{0,i}$ with (14). Collecting all terms up to quadratic order in the $b_{m,i}$ provides the effective Hamiltonian

$$H_{\text{eff}} = Jz \sum_{\mathbf{k} \in K} \vec{b}_{\mathbf{k}}^\dagger \begin{pmatrix} g_{11,\mathbf{k}}^{-1} & g_{12,\mathbf{k}}^{-1} & f_{11,\mathbf{k}}^{-1} & f_{12,\mathbf{k}}^{-1} \\ g_{21,\mathbf{k}}^{-1} & g_{22,\mathbf{k}}^{-1} & f_{21,\mathbf{k}}^{-1} & f_{22,\mathbf{k}}^{-1} \\ f_{11,\mathbf{k}}^{-1} & f_{12,\mathbf{k}}^{-1} & g_{11,\mathbf{k}}^{-1} & g_{12,\mathbf{k}}^{-1} \\ f_{21,\mathbf{k}}^{-1} & f_{22,\mathbf{k}}^{-1} & g_{21,\mathbf{k}}^{-1} & g_{22,\mathbf{k}}^{-1} \end{pmatrix} \vec{b}_{\mathbf{k}}, \quad (15)$$

where $\vec{b}_{\mathbf{k}} = (b_{1,\mathbf{k}}, b_{2,\mathbf{k}}, b_{1,-\mathbf{k}}^\dagger, b_{2,-\mathbf{k}}^\dagger)^\text{T}$ and K denotes the first Brillouin zone. We have dropped a constant term to be discussed later. The coefficients of the normal $g_{rs,\mathbf{k}}^{-1}$ and anomalous $f_{rs,\mathbf{k}}^{-1}$ terms are given in Appendix C. The appearance of anomalous terms in the effective Hamiltonian (15) is analogous to the situation where the corresponding spin problem is characterized by an antiferromagnetic ground state. These anomalous terms are removed via a Bogoliubov transformation which hybridizes creation and annihilation operators, thereby generating a new ground state carrying particle number fluctuations. This is in contrast to the ferromagnetic case, where the inclusion of quantum fluctuations does not impact on the classical ground state. The presence of the anomalous terms $f_{rs,\mathbf{k}}^{-1}$ away from $J = 0$ (cf. Appendix C), shows that the Mott-insulating state is ‘nonclassical’ and carries fluctuations for all finite values of J .

B. Diagonalization procedures

The diagonalization of the effective Hamiltonian (15) can be achieved via a (real) Bogoliubov transformation

$$M\vec{\beta}_{\mathbf{k}} = \vec{b}_{\mathbf{k}} \quad \text{with} \quad D = M^\text{T} H_{\text{eff}} M \quad (16)$$

diagonal, where $\vec{\beta}_{\mathbf{k}} = (\beta_{x,\mathbf{k}}, \beta_{y,\mathbf{k}}, \beta_{x,-\mathbf{k}}^\dagger, \beta_{y,-\mathbf{k}}^\dagger)^\text{T}$. In the Mott phase $x = p$ ($y = h$) stands for particle and hole excitations respectively, whereas in the superfluid phase these indices stand for sound ($x = s$) and massive ($y = m$)

modes. Those bosonic commutation relations that are not automatically fulfilled are imposed by the additional condition

$$M \Sigma M^\text{T} = \Sigma, \quad (17)$$

where the matrix Σ is given by the outer product

$$\Sigma \equiv (\vec{b}_{\mathbf{k}} \vec{b}_{\mathbf{k}}^\dagger)^\text{T} - (\vec{b}_{\mathbf{k}}^\dagger)^\text{T} (\vec{b}_{\mathbf{k}}) = \text{diag}(1, 1, -1, -1),$$

reminiscent of the metric tensor in Minkowski space. The group $O(2, 2)$, given by all real 4×4 -matrices M fulfilling (17), then shares many properties with the Lorentz group $O(1, 3)$, namely its decomposition in terms of ‘boosts’ (transformations of coordinates with different signs in the metric) and ‘rotations’ (transformations in a sector of the metric with equal signs). It turns out that this decomposition provides a useful strategy for the diagonalization of H_{eff} in the Mott phase, where the symmetries of H_{eff} allow for an efficient determination of the corresponding rapidities and angles. On the other hand, in the superfluid phase, these symmetries are absent and the diagonalization of H_{eff} is preferably done by mapping (16) and (17) to a non-Hermitian eigenvalue problem.³³

(I) In the Mott state ($\sigma = 0$, $\vartheta = 0$), where no anomalous mixing terms $f_{12,\mathbf{k}}^{-1} = f_{21,\mathbf{k}}^{-1} = 0$ between the $b_{1,\mathbf{k}}$ and the $b_{2,\mathbf{k}}$ bosons are present (see Appendix C), the parametrization of M in terms of boosts and rotations is suitable. To eliminate the anomalous terms $f_{11,\mathbf{k}}^{-1}$ and $f_{22,\mathbf{k}}^{-1}$ one chooses a boost in the $b_{m,\mathbf{k}}-b_{m,\mathbf{k}}^\dagger$ plane; a subsequent rotation in the $b_{1,\mathbf{k}}-b_{2,\mathbf{k}}$ plane leads to the mean-field dispersions⁸

$$\epsilon_{p(h)}(\mathbf{k}) = \mp[\epsilon_0(\mathbf{k})/2 + \delta\mu] + \tilde{\omega}(\mathbf{k}), \quad (18)$$

where $\tilde{\omega}(\mathbf{k}) = \sqrt{U^2 - U\epsilon_0(\mathbf{k})(4n_0 + 2) + \epsilon_0^2(\mathbf{k})}/2$ and $\epsilon_0(\mathbf{k}) = 2J \sum_{l=1}^d \cos(\mathbf{k} \cdot \mathbf{a}_l)$ is the bare band dispersion. Here, \mathbf{a}_l denote the vectors connecting nearest neighbors and we assume square and/or cubic symmetry, $a = |\mathbf{a}_l|$. The dispersions shown in Figs. 2(a) and (c) characterize two modes, describing particle and hole type excitations, both with nonvanishing gaps $\Delta_{p(h)} = \epsilon_{p(h)}(0)$, cf. Figs. 2(e) and (f). In the Mott phase, the relation between the $t_{\alpha,\mathbf{k}}$ and the $b_{m,\mathbf{k}}$ operators is trivial and the rotation in the $b_{1,\mathbf{k}}-b_{2,\mathbf{k}}$ plane takes us back to the $t_{\alpha,\mathbf{k}}$ operators. We therefore write the eigenstates in terms of the latter,

$$\beta_{p,\mathbf{k}}^\dagger = A(\mathbf{k})t_{1,\mathbf{k}}^\dagger + B(\mathbf{k})t_{-1,-\mathbf{k}}, \quad (19)$$

$$\beta_{h,\mathbf{k}}^\dagger = -A(\mathbf{k})t_{-1,\mathbf{k}}^\dagger - B(\mathbf{k})t_{1,-\mathbf{k}}, \quad (20)$$

with $A(\mathbf{k}) = \cosh(\text{arctanh}(f_{11,\mathbf{k}}^{-1}/g_{11,\mathbf{k}}^{-1})/2)$ and $B(\mathbf{k}) = \sinh(\text{arctanh}(f_{11,\mathbf{k}}^{-1}/g_{11,\mathbf{k}}^{-1})/2)$, where we have used the relations $g_{11,\mathbf{k}}^{-1} = g_{22,\mathbf{k}}^{-1}$ and $f_{11,\mathbf{k}}^{-1} = -f_{22,\mathbf{k}}^{-1}$, which apply for the Mott phase (cf. Appendix C).

(II) In the superfluid phase, the coefficients $f_{12,\mathbf{k}}^{-1}$ do not vanish and furthermore, $f_{11,\mathbf{k}}^{-1} \neq -f_{22,\mathbf{k}}^{-1}$. The presence of such terms renders a diagonalization via a parametrization of M as in the Mott state impractical.

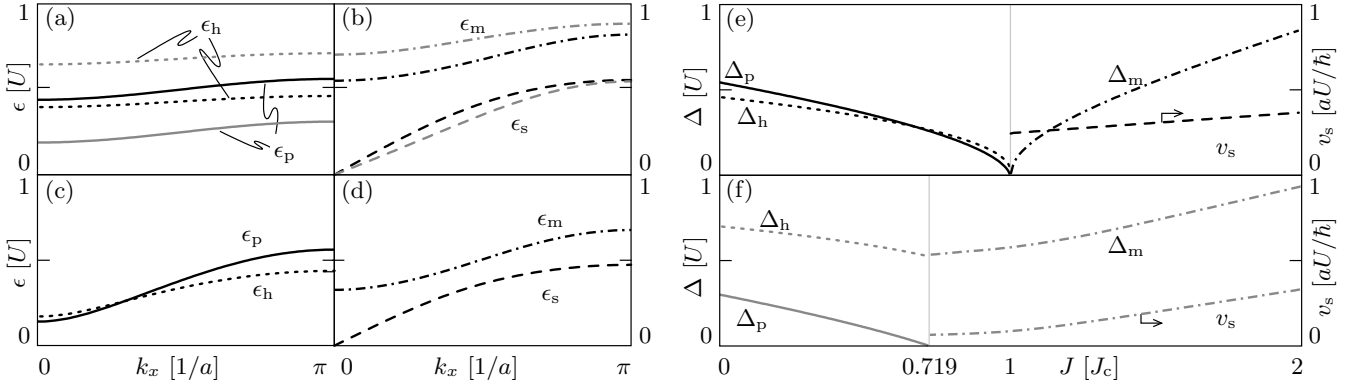


FIG. 2: The panels (a)-(d) show the spectra for different points in the phase diagram (cf. Fig. 1) in the $n_0 = 1$ lobe; all energies are measured in units of U . We display the results for the two-dimensional case with the dispersion along the direction k_x . Panel (a) and (c) refer to the Mott phase, with the full line corresponding to the particle branch and the dashed line to the hole branch. (a) $J = J_c/3$; black lines display dispersions on the line $\delta\mu_{n_0}$, gray lines correspond to $\delta\mu = 0.2U$; the change in chemical potential produces a shift in the spectra, cf. Eq. (18). (c) $J = 0.9 J_c$ and $\delta\mu = \delta\mu_{n_0}$; note the reduction in the gaps $\Delta_{p(h)}$ as compared to (a). Panels (b) and (d) refer to the superfluid phase with sound- and massive modes given by dashed and dash-dotted lines, respectively. (b) $J = 1.5 J_c$; black and gray lines refer to the chemical potentials $\delta\mu = \delta\mu_{n_0}$ and $\delta\mu = 0.2U$. (d) $J = 1.2 J_c$ closer to the transition and with $\delta\mu = \delta\mu_{n_0}$. Panels (e) and (f) give the gap values Δ_p , Δ_h , Δ_m and the sound velocity v_s for $J \in [0, 2J_c]$ and $\delta\mu = \delta\mu_{n_0}$ (e) and $\delta\mu = 0.2U$ (f). The value $J \approx 0.719 J_c$ corresponds to the phase boundary for $\delta\mu = 0.2U$ (cf. Fig. 1).

We therefore resort to the mapping onto a non-Hermitian eigenvalue problem.³³ The constraint (17) written as $M^T = \Sigma M^{-1} \Sigma$ and inserted into Eq. (16) yields

$$M^{-1} \Sigma H_{\text{eff}} M = \Sigma D, \quad (21)$$

The problem of finding a matrix $M \in \text{O}(2, 2)$ diagonalizing H_{eff} is now shifted to the problem of diagonalizing the non-Hermitian matrix ΣH_{eff} . The matrix M then is obtained from the eigenvectors $\{\tilde{v}\}$ of ΣH_{eff} via their proper normalization (with respect to Σ): let \tilde{M} be the matrix with columns $\{\tilde{v}\}$; then $M \in \text{O}(2, 2)$ is given by

$$M = L \tilde{M} \quad \text{where} \quad L = \text{diag}(l_1, l_2, l_3, l_4),$$

with

$$l_\alpha^{-2} = \left(\tilde{M} \Sigma \tilde{M}^T \right)_{\alpha\alpha}$$

(note that $\tilde{M} \Sigma \tilde{M}^T$ is diagonal, i.e., the eigenvectors $\{\tilde{v}\}$ are automatically orthogonal with respect to the metric Σ). After diagonalization the effective Hamiltonian reads

$$H_{\text{eff}} = \sum_{\mathbf{k} \in K} \epsilon_s(\mathbf{k}) \beta_{s,\mathbf{k}}^\dagger \beta_{s,\mathbf{k}} + \epsilon_m(\mathbf{k}) \beta_{m,\mathbf{k}}^\dagger \beta_{m,\mathbf{k}} - C_{J,U}^{\delta\mu}. \quad (22)$$

The optimization of the constant $C_{J,U}^{\delta\mu}$ leads to a renormalization of ϑ and σ and is discussed below. The eigenvalues $\epsilon_{s(m)}(\mathbf{k})$ can be calculated analytically (cf. Figs. 2(b) and (d)) and we find a sound (Goldstone) mode, which is linearly dispersing for $k \rightarrow 0$ with sound velocity $v_s = \partial_k \epsilon_s(k=0)/\hbar$ and a massive (Higgs) mode with a gap $\Delta_m = \epsilon_m(0)$, cf. Figs. 2(e) and (f). Note the

vanishing of the particle- and hole gaps and subsequent resurrection of the gap in the massive mode along the particle-hole symmetric line; for $\delta\mu > \delta\mu_{n_0}$ the hole gap transforms into the gap of the Higgs mode. The complete expressions for the dispersions of the sound and massive modes turn out to be lengthy and are given in Appendix C.

To further characterize the excitations we consider coherent states of sound $|\mathcal{B}_{s,\mathbf{q}}\rangle$ and massive modes $|\mathcal{B}_{m,\mathbf{q}}\rangle$, respectively,

$$|\mathcal{B}_{s(m),\mathbf{q}}\rangle = e^{-|\mathcal{B}_{s(m),\mathbf{q}}|^2/2} e^{\mathcal{B}_{s(m),\mathbf{q}} \beta_{s(m),\mathbf{q}}^\dagger} |0\rangle, \quad (23)$$

where $|0\rangle$ denotes the vacuum with respect to the $\beta_{s(m),\mathbf{q}}$ operators (i.e., the new ground state) and $\mathcal{B}_{s(m),\mathbf{q}} = |\mathcal{B}_{s(m),\mathbf{q}}| \exp[i\delta_{s(m),\mathbf{q}}]$ are complex numbers characterizing the coherent states. In Fig. 3 we present the expectation values of the density operator $\rho_i = \langle \mathcal{B}_{s(m),\mathbf{q}} | a_i^\dagger a_i | \mathcal{B}_{s(m),\mathbf{q}} \rangle$ and the order parameter $\psi_i = \langle \mathcal{B}_{s(m),\mathbf{q}} | a_i | \mathcal{B}_{s(m),\mathbf{q}} \rangle$ for $|\mathcal{B}_{s(m),\mathbf{q}}| \ll 1$ and \mathbf{q} along x with $q \ll \pi/a$, i.e., we only add a small amount of long wavelength excitations. The sound mode is given by a modulation of the phase accompanied by a modulation of the density, whereas the massive mode is given by a local conversion of condensate and noncondensate. In an effective theory for the order parameter ψ_i , the sound mode corresponds to the Goldstone mode, whereas the massive mode corresponds to the Higgs boson. The latter is only accessible for an effective theory which is second order in time. In Ref. 34, the author develops such an action for the superfluid to Mott-insulator phase transition.

The eigenvectors can be calculated analytically as well, however, for our purpose the numerical solution of (21)

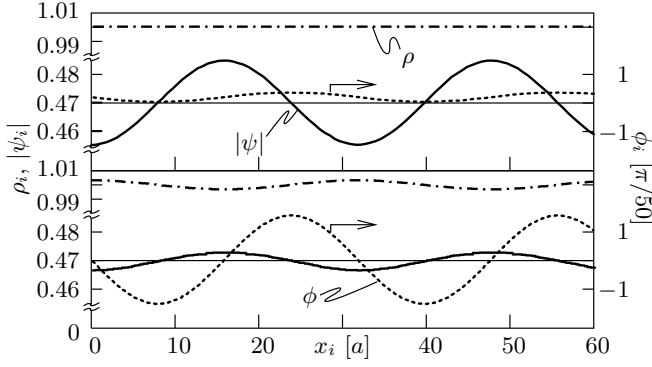


FIG. 3: Expectation values for the modulus $|\psi_i|$ and the phase $\phi_i = \arg(\psi_i)$ of the order parameter and the total density ρ_i for a coherent state of a massive mode (upper panel) and of a sound mode (lower panel). We have chosen parameters $n_0 = 1$, $J = 1.2J_c$, $\delta\mu = \delta\mu_{n_0}$ guaranteeing particle-hole symmetry, resulting in a ground-state order parameter $\psi_0 \approx 0.47$ marked by the faint gray line. Both modes refer to a \mathbf{q} value along x and $q \ll \pi/a$. The massive mode is given by a local conversion of condensate and noncondensate at fixed density, whereas the sound mode modulates the phase with a corresponding modulation of the density. In order to bring $|\psi_i|$ (ϕ_i) in both panels in registry we have chosen a phase difference $\delta_{s,q} - \delta_{m,q} = \pi/2$.

is preferable. Hermiticity allows us to write the transformation M in the form

$$M(\mathbf{k}) = \begin{pmatrix} N(\mathbf{k}) & P(\mathbf{k}) \\ P(-\mathbf{k}) & N(-\mathbf{k}) \end{pmatrix}; \quad (24)$$

in addition, inversion symmetry renders the elements of the 2×2 matrices $N(\mathbf{k})$ and $P(\mathbf{k})$ independent of the sign of \mathbf{k} and we can write

$$b_{1,\mathbf{k}}^\dagger = N_{11}(\mathbf{k})\beta_{m,\mathbf{k}}^\dagger + N_{12}(\mathbf{k})\beta_{s,\mathbf{k}}^\dagger + P_{11}(\mathbf{k})\beta_{m,-\mathbf{k}} + P_{12}(\mathbf{k})\beta_{s,-\mathbf{k}}, \quad (25)$$

$$b_{2,\mathbf{k}}^\dagger = N_{21}(\mathbf{k})\beta_{m,\mathbf{k}}^\dagger + N_{22}(\mathbf{k})\beta_{s,\mathbf{k}}^\dagger + P_{21}(\mathbf{k})\beta_{m,-\mathbf{k}} + P_{22}(\mathbf{k})\beta_{s,-\mathbf{k}}. \quad (26)$$

The matrices $N(\mathbf{k})$ and $P(\mathbf{k})$ are calculated numerically and all quantities of interest, e.g., response functions, are given in terms of $N_{ij}(\mathbf{k})$ and $P_{ij}(\mathbf{k})$.

The constant term

$$C_{J,U}^{\delta\mu} = Jz \sum_{\mathbf{k} \in K} g_{22,\mathbf{k}}^{-1} + g_{11,\mathbf{k}}^{-1} - (\epsilon_s(\mathbf{k}) + \epsilon_m(\mathbf{k}))/2 \quad (27)$$

needs further discussion. The shift can be interpreted as a fluctuation-induced reduction of the ground-state energy. In order to arrive at a self-consistent description, the parameters ϑ and σ have to be determined by the new condition that the energy shift $C_{J,U}^{\delta\mu}$ is maximal. This corresponds to finding a new density and superfluid density for a given set of parameters $J, U, \delta\mu$. Only if ϑ and σ are renormalized with respect to their mean-field values do we obtain a gapless sound mode, as demanded for

the broken-symmetry phase. In the Mott phase, $C_{J,U}^{\delta\mu}$ is not vanishing, but has its maximum again at $\vartheta = \sigma = 0$, thus generating no renormalization.

C. Validity and expectation values

The above method involves two approximations. First, the truncation of the Hilbert space: the quality of the truncation is expected to be acceptable in the Mott-insulating state and in the superfluid phase nearby, and turns bad in the weakly interacting limit. The quality of the approximation can be checked through comparison with experimental and numerical results, e.g., through testing the local number fluctuations. The latter have been measured³⁵ and found to be suppressed due to strong interactions, at least in the vicinity of the Mott phase. The data is consistent with subpoissonian number statistics as predicted in Ref. 36 and supports the validity of the truncation to three local states.³¹ The technique allows for systematic improvement by the inclusion of further local states.³⁷

Second, while the expansion of the constraint (14) is not *a priori* valid, we can check its quality via the (*a posteriori*) calculation of the ground state expectation values $\langle b_{m,i}^\dagger b_{m,i} \rangle$: we have found values in the range from 0.18 ($\bar{J} \rightarrow \infty$) to 0.21 ($\bar{J} = \bar{J}_c$); fluctuations are largest at the phase transition and go to zero in the Mott phase at $J \rightarrow 0$ for $n_0 = 1$ which justify our expansion in (14).

The calculation of matrix elements involves both states and the physical operator in question: so far, we have calculated the spectrum within the truncated Hilbert space, providing us with eigenvalues and eigenvectors of H_{eff} . In addition, we need to express the operators in the eigenbasis generated by the β operators. The specific step of replacing ‘Schwinger bosons’ by ‘Holstein-Primakoff’ type operators involves the elimination of all $b_{0,i}$ operators. Depending on the physical quantity under consideration, its expression through the β operators may or may not involve an expansion of the square root (14); in particular, the operators involving only $b_{1,i}$, $b_{2,i}$, and $n_{0,i} = b_{0,1}^\dagger b_{0,1}$ (e.g., the density operator in the Mott-insulating phase) can be transformed without requiring such an expansion. Otherwise, an additional imprecision has to be accepted due to the square root expansion of the constraint.

III. RESPONSE FUNCTIONS

While cold atoms in optical lattices excel in their tunability, they do suffer from a limited number of tools available for their characterization. In fact, so far only two experimental techniques are being used to determine the dynamical properties of cold atoms in an optical lattice, Bragg spectroscopy²⁷ and lattice modulation²². In Bragg spectroscopy, two laser beams are focused on the

system at an angle, leading to an inelastic two-photon scattering process. The system's response is described by the dynamic structure factor (density correlator)

$$S(\mathbf{q}, \omega) = \sum_n |\langle n | \delta\rho_{-\mathbf{q}} | 0 \rangle|^2 \delta(\hbar\omega - \hbar\omega_{n0}), \quad (28)$$

where $\delta\rho_{\mathbf{q}}$ is the density-fluctuation operator. The sum in (28) is running over all eigenstates $|n\rangle$ of the system with $|0\rangle$ denoting the ground state and $\hbar\omega_{n0}$ the excitation energy associated with $|n\rangle$. This method provides angle-resolved information on the system, a feature which, however, turns out to be responsible for the method's limitation in actual experiments, as the optical access to the atom cloud is usually restricted.

In the lattice modulation technique, recently introduced by Stöferle *et al.*, the depth of the optical lattice is modulated with a frequency ω , introducing side bands in the laser forming the optical lattice. Within the framework of the Bose-Hubbard model (1), the lattice modulation corresponds to a modulation in the hopping parameter J ; the determination of the energy transfer then boils down to a calculation of the hopping correlator

$$S_{(x)}^{\text{kin}}(\omega) = \sum_n |\langle n | T_{(x)} | 0 \rangle|^2 \delta(\hbar\omega - \hbar\omega_{n0}), \quad (29)$$

with $T_{(x)} = \sum_{\langle i,j \rangle_{(x)}} a_i^\dagger a_j$ the hopping operator (the index x refers to a restriction of the modulation along one direction, here the x axis). The energy absorption rate then is proportional to $\omega S(\mathbf{q}, \omega)$ and $\omega S_{(x)}^{\text{kin}}(\omega)$, respectively. In order to evaluate the response functions (28) and (29) we have to express the operators $\delta\rho_{\mathbf{q}}$ and $T_{(x)}$ in terms of the β bosons, involving a first transformation to b bosons and subsequent elimination of $b_{0,i}$, cf. Sec. II C.

We first concentrate on Bragg spectroscopy in the Mott and superfluid phases. In the Mott phase, where the local density is pinned to an integer value in the ground state, we expect to excite a particle-hole continuum spread in energy as described by the bandwidth of these two-particle excitations. Surprisingly, we find pronounced peaks within this continuum which we can relate to the single-mode excitations $\Delta_{h(p)+\epsilon_{p(h)}}(\mathbf{k})$. In the superfluid phase one expects single-mode excitations, as breaking the $U(1)$ symmetry is leading to collective excitations, and their weights will be determined.

Second, we proceed with the calculation of the hopping correlator $S_{(x)}^{\text{kin}}(\omega)$ in both the Mott-insulating and the superfluid phase. Again we find a continuum in the insulating phase. In the superfluid phase we do not expect to pump energy into the sound mode, as no momentum is transferred with this probe (up to a reciprocal lattice vector). A signal at finite energy will then give direct access to the massive mode.

A. Structure factor in the Mott phase

We make use of the eigenstates obtained within the variational mean-field approach to calculate the dynamic structure factor (28) in the Mott phase. In the truncated space the density-fluctuation operator

$$\delta\rho_{\mathbf{q}} = \sum_i (a_i^\dagger a_i - \langle a_i^\dagger a_i \rangle) e^{-i\mathbf{q} \cdot \mathbf{r}_i} \quad (30)$$

takes the form

$$\delta\rho_{\mathbf{q}} = \sum_{\mathbf{k} \in K} t_{1,\mathbf{k}}^\dagger t_{1,\mathbf{k}+\mathbf{q}} - t_{-1,\mathbf{k}}^\dagger t_{-1,\mathbf{k}+\mathbf{q}}, \quad (31)$$

where we have used the *exact* constraint (7) to eliminate $t_{0,i}$ ($= b_{0,i}$ in the Mott phase). Going over to β operators we obtain

$$\delta\rho_{\mathbf{q}} = \sum_{\mathbf{k} \in K} A(\mathbf{k}) B(\mathbf{k} + \mathbf{q}) [\beta_{p,\mathbf{k}}^\dagger \beta_{h,-(\mathbf{k}+\mathbf{q})}^\dagger - \beta_{h,\mathbf{k}}^\dagger \beta_{p,-(\mathbf{k}+\mathbf{q})}^\dagger]$$

and inserting this expression into the formula for the dynamic structure factor yields

$$S(\mathbf{q}, \omega) = \frac{1}{2} \int_K \frac{d\mathbf{k}}{v_0} P(\mathbf{k}, \mathbf{q}) \delta[\hbar\omega - \epsilon_h(\mathbf{k}) - \epsilon_p(\mathbf{q} - \mathbf{k})], \quad (32)$$

with $v_0 = (2\pi/a)^d$ the volume of the Brillouin zone. The matrix element $P(\mathbf{k}, \mathbf{q})$ quantifies the coupling of each particle-hole excitation to the density perturbation and is given by

$$1 + P(\mathbf{k}, \mathbf{q}) = \frac{\epsilon_0(\mathbf{k})\epsilon_0(\mathbf{q} - \mathbf{k}) + U^2 - U(2n_0 + 1)[\epsilon_0(\mathbf{k}) + \epsilon_0(\mathbf{q} - \mathbf{k})]}{4\tilde{\omega}(\mathbf{k})\tilde{\omega}(\mathbf{q} - \mathbf{k})}. \quad (33)$$

The dynamic structure factor (32) is closely related to the two-particle density of states (2DOS) given by

$$D(\mathbf{q}, \omega) = \int_K \frac{d\mathbf{k}}{v_0} \delta[\hbar\omega - \epsilon_h(\mathbf{k}) - \epsilon_p(\mathbf{q} - \mathbf{k})]. \quad (34)$$

They share the same bandwidth as well as the characteristic total gap of the insulating state

$$\Delta_{\text{tot}} = \Delta_p + \Delta_h = \sqrt{U^2 - 2JzU(2n_0 + 1) + (Jz)^2}. \quad (35)$$

Moreover, the van Hove singularities present in the 2DOS influence the response function, see Fig. 4(b).

In our discussion of the results,³⁸ see Figs. 4(a) and (b), we concentrate on the two-dimensional situation where our mean-field analysis is sufficiently accurate. In the Mott phase, particle-hole excitations lead to a continuum, starting with a finite gap Δ_{tot} at zero momentum \mathbf{q} . The bandwidth decreases with increasing momentum transfer following the support of the 2DOS and reaches a minimum at the zone boundary, see Fig. 4(a). Figure 4(b) shows the 2DOS $D(\mathbf{q}, \omega)$ as well as $S(\mathbf{q}, \omega)$ at $\mathbf{q} = (0.9\pi/a)\mathbf{e}_x$. The van Hove singularities in the 2DOS are

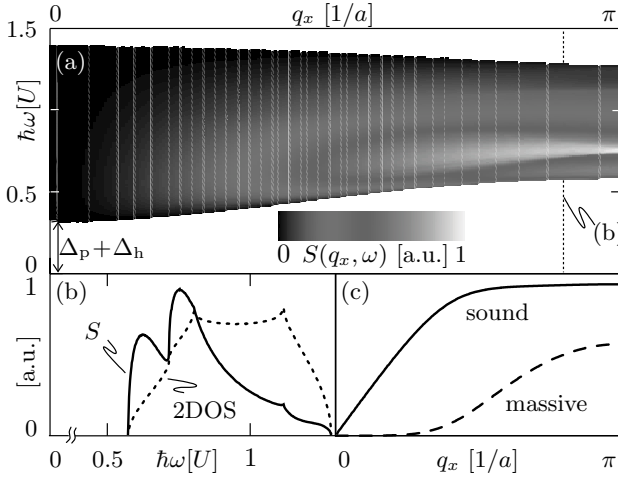


FIG. 4: (a) Density plot of the dynamic structure factor $S(\mathbf{q}, \omega)$ in the Mott phase along q_x for $J = 0.9J_c$ [point (c) in Fig. 1, energies are measured in units of U and $n_0 = 1$, the chemical potential $\delta\mu$ has no influence on the structure factor]. The spectrum is gapped, the spectrum's bandwidth decreases towards the zone edge, while at the same time developing a pronounced structure allowing for the identification of single-mode excitations. (b) Cut along the ω direction at $q_x = 0.9\pi/a$ [dotted line in (a)]. The dynamic structure factor (solid line) exhibits marked peaks at the single-mode energies; the dotted line shows the 2DOS exhibiting van Hove singularities. (c) Single-mode weights of dynamic structure factor $S(\mathbf{q}, \omega)$ in the superfluid phase at $J = 1.2J_c$ and $\delta\mu = \delta\mu_{n_0}$. The sound mode (Goldstone, solid line) exhausts all the available spectral weight at long wavelengths, allowing the massive mode (Higgs, dashed line) to gain weight only towards the zone boundary ([a.u.] denotes 'arbitrary units').

washed out in the response function which is dominated by the matrix element $P(\mathbf{k}, \mathbf{q})$. The latter generates the two pronounced peaks in $S(\mathbf{q}, \omega)$ which we find (numerically) to be located at $\Delta_p + \epsilon_h(q_x)$ and $\Delta_h + \epsilon_p(q_x)$. Hence, although Bragg spectroscopy generically excites a two-particle continuum, tracing these peaks allows for the extraction of the single-particle energies. These peaks are most prominent near the zone boundary and can be enhanced at small values of q_x by dividing out a global modulation of the form $[1 - \cos(q_x/a)]$ (cf. Appendix B) from $S(\mathbf{q}, \omega)$. Furthermore, the peaks disappear deeper in the Mott phase where the excitations are more localized. We note that by expanding the integral (32) in J/U , we recover the results of the perturbative treatment (see Appendix B), hence the quadratic expansion of the constraint (7) is consistent with second-order perturbation theory; however, the two results are comparable only for $J \lesssim 10^{-2}J_c$.

B. Structure factor in the superfluid phase

In the superfluid phase, the expression for the density fluctuation operator (31) written in terms of the b bosons contains $b_{0,i}$ operators, which have to be removed via an expansion of the square root (14), leading to terms linear in the operators $b_{m,\mathbf{k}}^\dagger$ as well as higher-order terms. Going over to β operators we obtain the expression

$$\delta\rho_{\mathbf{q}} = \sin(\vartheta/2) \left\{ [P_{21}(\mathbf{q}) + N_{21}(\mathbf{q})]\beta_{m,\mathbf{q}}^\dagger [P_{22}(\mathbf{q}) + N_{22}(\mathbf{q})]\beta_{s,\mathbf{q}}^\dagger \right\} + O(\beta^2). \quad (36)$$

Accounting only for terms up to first order, we ignore two- and multiparticle excitations and we cannot expect to fulfill the f -sum rule exactly, see the discussion in Sec. III C below. Inserting (36) into the expression for the dynamic structure factor yields

$$\frac{1}{N}S^{(1)}(\mathbf{q}, \omega) = \sin^2(\vartheta/2) \left[\tilde{S}^2(\mathbf{q})\delta(\hbar\omega - \epsilon_s(\mathbf{q})) + \tilde{M}^2(\mathbf{q})\delta(\hbar\omega - \epsilon_m(\mathbf{q})) \right]; \quad (37)$$

this result reveals the two collective modes (22) characterizing the superfluid phase. Their weights are given by $\tilde{M}(\mathbf{q}) = P_{21}(\mathbf{q}) + N_{21}(\mathbf{q})$ for the massive mode and $\tilde{S}(\mathbf{q}) = P_{22}(\mathbf{q}) + N_{22}(\mathbf{q})$ for the sound mode and are shown in Fig. 4(c). The sound mode is dominating the response at low momenta, with the massive mode acquiring weight only for higher momenta, where the sound mode saturates; in fact, numerical analysis confirms $\propto q^4$ dependence of $\tilde{M}^2(\mathbf{q})$ at small \mathbf{q} .

Besides the single mode contribution, $\delta\rho_{\mathbf{q}}$ also yields two-particle continua involving the excitations $|m, \mathbf{k}; s, \mathbf{q} - \mathbf{k}\rangle$, $|m, \mathbf{k}; m, \mathbf{q} - \mathbf{k}\rangle$ and $|s, \mathbf{k}; s, \mathbf{q} - \mathbf{k}\rangle$. Their weight is about three orders of magnitude smaller than the single-particle contribution, however.

C. Particle-number conservation

The dynamic structure factor is constrained by several sum rules deriving from conservation laws. Gauge symmetry and thus particle-number conservation is leading to the well known f -sum rule

$$\int_0^\infty d\omega \omega S(\mathbf{q}, \omega) = \frac{Nq^2}{2m}, \quad (38)$$

which is modified in a one-band lattice description. The broken translational symmetry is leading to a nonquadratic dispersion, which can be characterized by a \mathbf{k} -dependent effective mass tensor $\hbar^2/m_{ij}^*(\mathbf{k}) = \partial_{k_i} \partial_{k_j} \epsilon_0(\mathbf{k})$. The f -sum rule^{29,39} adapted to the pres-

ence of a lattice then takes the form

$$\begin{aligned}
 & \int_0^\infty d\omega \omega S(\mathbf{q}, \omega) \\
 &= \frac{1}{2\hbar^2} \sum_{\mathbf{k} \in K} \{ \epsilon_0(\mathbf{k} + \mathbf{q}) + \epsilon_0(\mathbf{k} - \mathbf{q}) - 2\epsilon_0(\mathbf{k}) \} \langle 0 | a_{\mathbf{k}}^\dagger a_{\mathbf{k}} | 0 \rangle \\
 &\stackrel{q \rightarrow 0}{\approx} \sum_{ij} \frac{q_i q_j}{2} \sum_{\mathbf{k} \in K} \frac{\langle 0 | a_{\mathbf{k}}^\dagger a_{\mathbf{k}} | 0 \rangle}{m_{ij}^*(\mathbf{k})} \\
 &\quad \left(= \frac{Nq^2}{2m} \quad \text{for} \quad \frac{1}{m_{ij}^*(\mathbf{k})} \equiv \frac{1}{m} \delta_{ij} \right).
 \end{aligned} \tag{39}$$

Unlike in translation-invariant systems the structure of the ground state enters the f -sum rule via the nonuniversal prefactor

$$I_{ij}(J/U) = \sum_{\mathbf{k} \in K} \frac{\langle 0 | a_{\mathbf{k}}^\dagger a_{\mathbf{k}} | 0 \rangle}{m_{ij}^*(\mathbf{k})}. \tag{40}$$

The expression (39) predicts $\propto q^2$ behavior at small q , which is trivially fulfilled in the superfluid phase (combine the weight $\tilde{S}^2 \propto q$, see Fig. 4(c), with the linear dispersion of the sound mode; the $\propto q^4$ dependence of \tilde{M}^2 does not contribute at small q) and can be easily verified in the Mott phase via expansion of the matrix element $P(\mathbf{k}, \mathbf{q})$,

$$P(\mathbf{q}, \mathbf{k}) = P^{(2)}(\mathbf{k})q^2 + O(q^4).$$

Unfortunately, our scheme does not allow for a precise calculation of the prefactor (40) and hence an exact self-consistency check (via particle-number conservation) of our result is not possible.

The issue of number conservation has been raised in the work of van Oosten *et al.*²⁸. Their field-theoretic calculation of the structure factor did not reproduce the required q^2 behavior, which then has been enforced through the use of Ward identities. However, it appears that the Green's function⁸ $G(i\omega_n, \mathbf{k})$ used in this calculation already violates number conservation in the Mott phase, i.e.

$$\rho_i = \langle n_i \rangle = \frac{1}{\beta} \sum_{i\omega_n} \int_K \frac{d\mathbf{k}}{v_0} G(i\omega_n, \mathbf{k}) \neq n_0.$$

The application of Ward identities, although guaranteeing number conservation, generates other defects in the structure factor, e.g., the appearance of linear terms in J spoiling the $J \rightarrow -J$ symmetry present in bipartite lattice models.

D. Lattice modulation in the Mott phase

The lattice-depth modulation is a particle-number conserving probe and hence produces only particle-hole excitations. While the lattice modulation has been uniaxial

so far,²² here, we also discuss its extension to an isotropic modulation (we discuss the case of equal modulation amplitudes but allow for mutual phase-differences between the various directions). Expanding the constraint to second (i.e., leading) order, we obtain the response function⁴⁰

$$S_{(x)}^{\text{kin}}(\omega) = \frac{1}{2} \int_K \frac{d\mathbf{k}}{v_0} P_{(x)}^{\text{kin}}(\mathbf{k}) \delta[\hbar\omega - \epsilon_h(\mathbf{k}) - \epsilon_p(-\mathbf{k})], \tag{41}$$

with

$$P_{(x)}^{\text{kin}}(\mathbf{k}) = 2n_0(n_0 + 1) |\Sigma_{(x)}(\mathbf{k})|^2 \left[\frac{U}{\tilde{\omega}(\mathbf{k})} \right]^2. \tag{42}$$

The interference generated by the different lattice modulations is encoded in the sum

$$\Sigma(\mathbf{k}) = 2 \sum_{l=1}^d e^{i\phi_l} \cos(\mathbf{k} \cdot \mathbf{a}_l); \tag{43}$$

for the uniaxial modulation this reduces to

$$\Sigma_x(\mathbf{k}) = 2 \cos(\mathbf{k} \cdot \mathbf{a}_x). \tag{44}$$

The relative phase ϕ_l between the different lattice modulations can lead to interesting interference effects, see below.

In Figs. 5(b) and (c) the results for isotropic and uniaxial lattice modulation are shown for $\phi_l = 0$ and $d = 2$. The bandwidth is determined by the 2DOS (34) at zero momentum transfer \mathbf{q} . Energy is transferred to the system only at frequencies ω above the gap $\Delta_{\text{tot}}/\hbar$, offering a simple way to determine the gap value. A dramatic change is obtained when going from the uniaxial to the isotropic modulation: the cusp at $\hbar\omega = U$ disappears and is replaced by a zero in the absorption probability. As the matrix element $P^{\text{kin}}(\mathbf{k})$ is non-negative, the response (41) only disappears if $P^{\text{kin}}(\mathbf{k}) \equiv 0$ for all \mathbf{k} -values on the line defined by the δ -function in the integral (41). At nonzero ϕ_l , a finite weight is assembled away from the points $(\pm\pi/2, \pm\pi/2)$, leading to a finite response at $\omega = U$. However, for $\phi_l \ll \pi$ an appreciable suppression is still observable.

The result (41) obtained here has to be compared with the one obtained by Iucci and coworkers:²⁵ in their perturbative calculation the factor $[U/\tilde{\omega}(\mathbf{k})]^2$ does not show up. Instead, the Bogoliubov transformation used here is equivalent to a resummation of diagrams and leads to this factor generating the interesting structure in the response function (41).

Comparing our result with the experiment of Stöferle *et al.*²² we have to consider the uniaxial case, i.e., $S_x^{\text{kin}}(\omega)$. While Stöferle *et al.* observe a broad two-peak structure with maxima around U and $2U$, the present accuracy of our calculation does not account for high-energy excitations residing around $2U$. On the other hand, the current experimental resolution does not allow to trace the interesting structure on the scale of the bandwidth, see Figs. 5(b) and (c). Thus, both theory and experiment have to

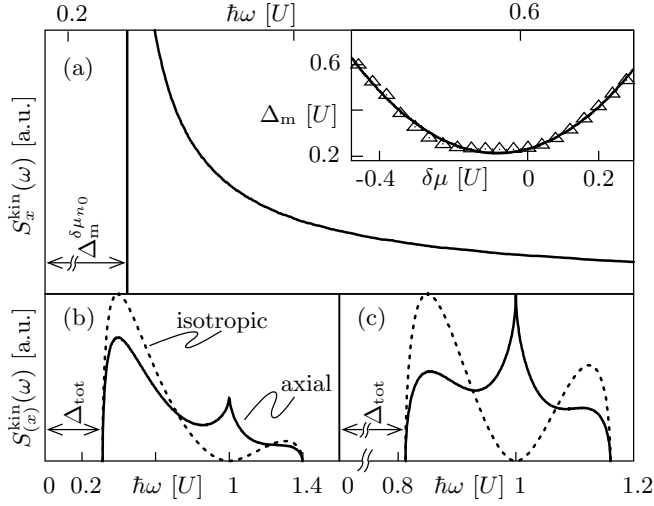


FIG. 5: (a) Hopping correlator $S_x^{\text{kin}}(\omega)$ in the superfluid phase for $J = 1.2J_c$ and $n_0 = 1$ for a parabolic trap and commensurate filling in the center (in a homogeneous system the response is nonzero only at $\omega = \Delta_m$). The inset shows the gap Δ_m of the massive mode as a function of the chemical potential with a minimum at commensurate filling $\delta\mu = \delta\mu_{n_0}$. The triangles are the calculated gap values and the solid line is a fit used in the calculation of $S_x^{\text{kin}}(\omega)$ in a trap. (b) $S_x^{\text{kin}}(x)$ in the Mott phase at $J = J_c/3$. The response consists of a particle-hole continuum with a gap Δ_{tot} . The striking difference between the uniaxial [$S_x^{\text{kin}}(\omega)$, solid line] and the isotropic [$S_x^{\text{kin}}(x)$, dashed line] situation is due to interference effects. (c) The same as in (b) for $J = 0.9J_c$, where the gap Δ_{tot} is larger and the available bandwidth smaller.

be developed further in order to allow for a precise comparison. Furthermore, it is worth mentioning that the current experiment may probe non-linear response.⁴¹

E. Lattice modulation in the superfluid phase

In the superfluid phase (with an order parameter $|\psi| > 0$), the expansion of the constraint again provides terms linear in the β operators and we obtain single mode peaks in the hopping correlator S_x^{kin} at $\hbar\omega = 0$ and $\hbar\omega = \Delta_m$ due to sound and massive excitations, respectively. Energy absorption is due to the excitation of the massive mode only and its weight $W_{\text{mass}} \propto |\psi|^2$ is given in Appendix C. In addition, we also find a two-mode continuum (dominated by processes $|s, \mathbf{k}; m, -\mathbf{k}\rangle$) with a weight suppressed by more than three orders of magnitude in the entire parameter range.

In a trap, the sharp peak at Δ_m will be smeared due to the inhomogeneous density distribution. [Note that in the Mott phase, the response is not changed by the trap as both excitation energies $\epsilon_h(\mathbf{k}) + \epsilon_p(\mathbf{q} - \mathbf{k})$ (18) and the matrix elements $P(\mathbf{k}, \mathbf{q})$ and $P_{(x)}^{\text{kin}}(\mathbf{k})$ are independent of $\delta\mu$]. The onset of absorption is determined by the minimal gap Δ_m^{min} which occurs on the particle-hole

symmetric line $\delta\mu = \delta\mu_{n_0}$ and the shape of the absorption profile depends on the distribution of effective chemical potentials $\mu_{\text{eff}}(r) = \mu - V_{\text{trap}}(r)$ in the trap. Here, we analyze the shape for a quadratic trap with $\mu_{\text{eff}}(0) = \delta\mu_{n_0}$ for a superfluid close to the Mott phase, $J = 1.2J_c$. The dependence of the gap Δ_m on the chemical potential $\delta\mu$ can be calculated, see the inset of Fig. 5(a), and a convenient fit is given by $\Delta_m - \Delta_m^{\text{min}} = w(\delta\mu - \delta\mu_{n_0})^2$ with $w \approx 2.06U^{-1}$. The hopping correlator then draws its weight at frequency ω from rings matching the local gap energy $\Delta_m(r)$,

$$S_x^{\text{kin}}(\omega) = \frac{1}{\pi R^2} \int_0^R dr 2\pi r W_{\text{mass}} \delta[\hbar\omega - \Delta_m(r)] \propto \frac{1}{\sqrt{\hbar\omega - \Delta_m^{\text{min}}}} \quad \text{for } \hbar\omega > \Delta_m^{\text{min}}. \quad (45)$$

The resulting tail then resembles the broad absorption profile observed in the experiment of Stöferle *et al.*^{22,42} Note that the precise shape depends on the actual density distribution in the trap; in particular, the divergence at Δ_m^{min} is removed when $\mu_{\text{eff}}(0) \neq \delta\mu_{n_0}$. Another potential source of broadening is the finite lifetime of the massive mode due to the decay into two phonons as considered by Altman and Auerbach in Ref. 31. However, in two and more dimensions the effect of the trap dominates over the lifetime broadening.

IV. SUMMARY AND CONCLUSIONS

We have generalized the truncation scheme, introduced by Altman and Auerbach³¹ to deal with the Bose-Hubbard model in the particle-hole symmetric limit (large particle numbers $n_0 \gg 1$), to the experimentally relevant situation of small filling numbers n_0 of order unity. The determination of excitations consisting of small fluctuations about a variational ground state is inspired by the Holstein-Primakoff description of quantum-spin systems and corresponds to the determination of spin-wave excitations above an antiferromagnetic ground state.⁴³ We have determined the mean-field phase diagram as well as the spectra and eigenstates in the Mott-insulator and superfluid phases. These results then have been applied to the calculation of two response functions, the structure factor (density correlator) describing Bragg spectroscopy and the hopping correlator describing the lattice-modulation spectroscopy.

A mean-field variational ansatz provides us with the usual phase diagram valid in dimensions $d \geq 2$. The inclusion of two additional levels allows us to account for particle and hole-type excitations in the Mott phase and we determine, using a Bogoliubov transformation, the dispersions of the two gapped modes; at the same time, the Bogoliubov transformation introduces a new ground state carrying particle-hole fluctuations. In the superfluid phase, we find a sound (Goldstone) and a massive (Higgs) mode and we determine the characteristic veloc-

ity and gap parameters. The massive mode describes a local counterflow of condensate and normal densities; this mode is absent in a Gross-Pitaevskii description where the dynamics involves a first-order time derivative, but is allowed in a Klein-Gordon type theory with a second-order dynamics. The presence of the latter is due to the underlying Mott physics providing ‘particles’ and ‘anti-particles’ (holes) and has been shown to be relevant in the Mott-insulator–superfluid transition in Ref. 21 (an additional first-order derivative is present away from the particle-hole symmetric line). A similar (massive) mode was found for the charge-density-wave compound NbSe₂ below the superconducting transition temperature.^{46,47} The fate of this gapped mode for $U \rightarrow 0$, where higher occupation numbers are of importance, is currently under investigation.³⁷

In the Mott phase, Bragg spectroscopy excites a particle-hole continuum and provides information on the gap and bandwidth of these two-particle excitations. To our surprise, we find that the structure factor unveils the single-particle excitation energies as well. In the superfluid phase, collective modes (sound and massive) are excited and visible as sharp peaks (to be smeared in a trap); the massive mode gains weight only at large momenta. The transition can be traced watching the appearance of a gap when crossing from the superfluid into the Mott-insulating phase.

The lattice-modulation scheme²² is presently the tool of choice to gain spectroscopic information on atomic matter in optical lattices. Our calculation of the hopping correlator providing the system’s response reveals a two-particle continuum in the Mott phase which is sensitive to the details of the excitation scheme, uniaxial versus isotropic. The response in the superfluid is determined by the massive mode which appears as a sharp peak at finite frequencies. In order to better account for the experimental results we have extended our analysis to include the smearing due to the trap and find that the precise shape depends sensitively on the value of the chemical potential in the trap center. The experimental detection of such an energy absorption at finite frequency cannot be easily understood within a weakly interacting theory as described by the Gross-Pitaevskii equation. On the other hand, our strongly interacting theory provides a massive (Higgs) mode which naturally accounts for such a finite frequency absorption. Furthermore, a future experiment could address the question of how this Higgs mode disappears in the weakly interacting regime.

We thank A. Castro-Neto, T. Esslinger, M. Köhl, C. Kollath, F. Hassler, and A. Rüegg for discussions and the Swiss NSF for financial support via the NCCR MaNEP. The numerical work was performed on the Hreidar cluster at ETH Zürich. Work in Innsbruck was supported by the Austrian Science Foundation, and the Institute for Quantum Information.

APPENDIX A: SPIN HAMILTONIAN

Defining the spin-1 operators S_i^+ , S_i^- and S_i^z in terms of the $t_{\alpha,i}$ operators via

$$S_i^+ = \sqrt{2}(t_{1,i}^\dagger t_{0,i} + t_{0,i}^\dagger t_{-1,i}) \quad (\text{A1})$$

$$S_i^- = \sqrt{2}(t_{0,i}^\dagger t_{1,i} + t_{-1,i}^\dagger t_{0,i}) \quad (\text{A2})$$

$$S_i^z = t_{1,i}^\dagger t_{1,i} - t_{-1,i}^\dagger t_{-1,i} \quad \text{with} \quad (\text{A3})$$

$$[S_i^+, S_i^-] = 2S_i^z, \quad [S_i^z, S_i^\pm] = \pm S_i^\pm, \quad (\text{A4})$$

we can write the Bose Hubbard Hamiltonian (1) in the truncated space as

$$\begin{aligned} H_{\text{BH}}^{\text{spin}} = & -\frac{Jn_0}{2} \sum_{\langle i,j \rangle} S_i^+ S_j^- + \frac{U}{2} \sum_i (S_i^z)^2 - \delta\mu \sum_i S_i^z \\ & - \frac{Jn_0\xi}{2} \sum_{\langle i,j \rangle} [S_i^z S_i^+ S_j^- + S_i^- S_i^z S_j^+ + S_i^- S_j^z S_j^+ + S_i^+ S_j^- S_j^z \\ & + \xi(S_i^z S_i^+ S_j^- S_j^z + S_i^+ S_i^z S_j^- S_j^z)], \quad (\text{A5}) \end{aligned}$$

where $\xi = \sqrt{(n_0 + 1)/n_0} - 1$ is a measure of the ‘particle-hole symmetry-breaking’. In the work of Altman and Auerbach,³¹ ξ was set to zero.

APPENDIX B: PERTURBATION THEORY

For a perturbative treatment of the dynamic structure factor one starts from the *pure* Mott state $|\tilde{0}\rangle$ where all sites are occupied by exactly n_0 particles. A consistent expansion of (28) in J/U is obtained by an admixture of virtual particle hole pairs in the ground state

$$|0\rangle^{(1)} = -J \sum_{i \neq j} \sum_{\langle l,m \rangle} |i,j\rangle \frac{\langle i,j|a_l^\dagger a_m|\tilde{0}\rangle}{U} + |\tilde{0}\rangle, \quad (\text{B1})$$

where $|i,j\rangle$ denotes a state with $n_0 + 1$ particles at i and $n_0 - 1$ particles at j . The excited states in (28) are to lowest order given by the states

$$|n\rangle = |\mathbf{k}_p, \mathbf{k}_h\rangle = \frac{1}{N} \sum_{i \neq j} e^{i(\mathbf{k}_p \cdot \mathbf{r}_i - \mathbf{k}_h \cdot \mathbf{r}_j)} |i,j\rangle, \quad (\text{B2})$$

with the energies

$$\epsilon(\mathbf{k}_p, \mathbf{k}_h) = U - (n_0 + 1)\epsilon_0(\mathbf{k}_p) - n_0\epsilon_0(\mathbf{k}_h). \quad (\text{B3})$$

Inserting these perturbative states and energies into (28) leads to the expression

$$\begin{aligned} S^{(2)}(\mathbf{q}, \omega) = & N \left(\frac{J}{U} \right)^2 n_0(n_0 + 1) \times \\ & \int_{\text{K}} \frac{d\mathbf{k}}{v_0} [d\gamma(\mathbf{q} - \mathbf{k}) - d\gamma(\mathbf{k})]^2 \delta(\hbar\omega - \epsilon(\mathbf{q} - \mathbf{k}, \mathbf{k})), \quad (\text{B4}) \end{aligned}$$

where $\gamma(\mathbf{k}) = 1/z \sum_{l=1}^d \exp(i\mathbf{k} \cdot \mathbf{a}_l)$. Both sides of the f -sum rule can be calculated independently and they coincide with a value given by

$$\int_0^\infty d\omega \omega S^{(2)}(\mathbf{q}, \omega) = 4 \frac{J^2}{U} N d n_0 (n_0 + 1) \left[1 - \frac{1}{2} \gamma(\mathbf{q}) \right],$$

which shows again the quadratic dependence on J and the vanishing with q^2 for small \mathbf{q} .

APPENDIX C: EFFECTIVE HAMILTONIAN

1. Second order expansion

Replacing all operators $b_{0,i}$ in (1) expressed in the b -bosons and collecting all terms second order in $b_{1,i}$, $b_{2,i}$ is leading to the effective Hamiltonian

$$H_{\text{eff}} = 2Jz \sum_{\mathbf{k} \in K} g_{11,\mathbf{k}}^{-1} b_{1,\mathbf{k}}^\dagger b_{1,\mathbf{k}} + g_{22,\mathbf{k}}^{-1} b_{2,\mathbf{k}}^\dagger b_{2,\mathbf{k}} + \left(\frac{f_{11,\mathbf{k}}^{-1}}{2} b_{1,\mathbf{k}}^\dagger b_{1,-\mathbf{k}}^\dagger + \frac{f_{22,\mathbf{k}}^{-1}}{2} b_{2,\mathbf{k}}^\dagger b_{2,-\mathbf{k}}^\dagger + g_{12,\mathbf{k}}^{-1} b_{1,\mathbf{k}}^\dagger b_{2,\mathbf{k}} + f_{12,\mathbf{k}}^{-1} b_{1,\mathbf{k}}^\dagger b_{2,-\mathbf{k}}^\dagger + \text{H.c.} \right), \quad (\text{C1})$$

where we extracted a factor $2Jz$ corresponding to the non-interacting band-width from the definitions of the coefficients given by

$$\begin{aligned} g_{11,\mathbf{k}}^{-1} &= -\frac{\delta\mu}{2Jz} \sin(2\sigma) \cos(\vartheta) + \frac{U}{4Jz} \cos(\vartheta) + \frac{1}{2} [1 - \cos^2(\vartheta)] \{n + \sqrt{n(n+1)} \cos(2\sigma) + \frac{1}{2} [\sin(2\sigma) + 1]\} \\ &\quad - \frac{\gamma_{\mathbf{k}}}{2} \left\{ \frac{1}{2} [\cos^2(\vartheta) + 1] \{n + \frac{1}{2} [\sin(2\sigma) + 1]\} - \frac{1}{2} \sqrt{n(n+1)} [1 - \cos^2(\vartheta)] \cos(2\sigma) \right\}, \\ g_{22,\mathbf{k}}^{-1} &= +\frac{\delta\mu}{4Jz} [3 - \cos(\vartheta)] \sin(2\sigma) + \frac{U}{8Jz} [\cos(\vartheta) + 1] + \frac{1}{4} [1 - \cos^2(\vartheta)] \{n + \sqrt{n(n+1)} \cos(2\sigma) + \frac{1}{2} [\sin(2\sigma) + 1]\} \\ &\quad - \frac{\gamma_{\mathbf{k}}}{4} \left\{ n + \frac{1}{2} [1 - \sin(2\sigma)] \right\} [\cos(\vartheta) + 1], \\ g_{12,\mathbf{k}}^{-1} &= -\frac{\delta\mu}{2Jz} \cos(\vartheta/2) \cos(2\sigma) + \cos(\vartheta/2) \frac{1}{8} [1 - \cos(\vartheta)] [\cos(2\sigma) + 2\sqrt{n(n+1)} \sin(2\sigma)] \\ &\quad - \frac{\gamma_{\mathbf{k}}}{8} \cos(\vartheta/2) \left\{ [\cos(\vartheta) + 1] \cos(2\sigma) + 2\sqrt{n(n+1)} [1 - \cos(\vartheta)] \sin(2\sigma) \right\}, \\ f_{11,\mathbf{k}}^{-1} &= \frac{\gamma_{\mathbf{k}}}{4} \left\{ [1 - \cos^2(\vartheta)] \{n + \frac{1}{2} [\sin(2\sigma) + 1]\} - \sqrt{n(n+1)} [\cos^2(\vartheta) + 1] \cos(2\sigma) \right\}, \\ f_{22,\mathbf{k}}^{-1} &= \frac{\gamma_{\mathbf{k}}}{4} \sqrt{n(n+1)} [\cos(\vartheta) + 1] \cos(2\sigma), \\ f_{12,\mathbf{k}}^{-1} &= \frac{\gamma_{\mathbf{k}}}{8} \cos(\vartheta/2) \left\{ [1 - \cos(\vartheta)] \cos(2\sigma) + \sqrt{n(n+1)} [\cos(\vartheta) + 1] \sin(2\sigma) \right\}, \end{aligned} \quad (\text{C2})$$

where we defined again $\gamma(\mathbf{k}) = 1/z \sum_{l=1}^d \exp(i\mathbf{k} \cdot \mathbf{a}_l)$.

2. Dispersion in the superfluid phase

In the superfluid phase the excitation energies are given by

$$\epsilon_{s(m)}(\mathbf{k}) = Jz \sqrt{2 \left[A_\epsilon(\mathbf{k}) \mp \sqrt{A_\epsilon(\mathbf{k})^2 - 4B_\epsilon(\mathbf{k})} \right]}, \quad (\text{C3})$$

and the coefficients are defined as

$$\begin{aligned} A_\epsilon(\mathbf{k}) &= (g_{11,\mathbf{k}}^{-1})^2 + (g_{22,\mathbf{k}}^{-1})^2 - (f_{11,\mathbf{k}}^{-1})^2 - (f_{22,\mathbf{k}}^{-1})^2 + \\ &\quad 2(g_{12,\mathbf{k}}^{-1})^2 - 2(f_{12,\mathbf{k}}^{-1})^2, \\ B_\epsilon(\mathbf{k}) &= ((g_{11,\mathbf{k}}^{-1} - f_{11,\mathbf{k}}^{-1})(g_{22,\mathbf{k}}^{-1} - f_{22,\mathbf{k}}^{-1}) - (g_{12,\mathbf{k}}^{-1} - f_{12,\mathbf{k}}^{-1})^2) \times \\ &\quad ((g_{11,\mathbf{k}}^{-1} + f_{11,\mathbf{k}}^{-1})(g_{22,\mathbf{k}}^{-1} + f_{22,\mathbf{k}}^{-1}) - (g_{12,\mathbf{k}}^{-1} + f_{12,\mathbf{k}}^{-1})^2). \end{aligned}$$

3. Massive mode weight the hopping correlator

The weight W_{mass} of the delta peak at Δ_m in S^{kin} is given by

$$W_{\text{mass}} = \sin(\vartheta)^2 \left[\cos(\vartheta/2)^2 (N_{21}(0) + P_{21}(0)) - \frac{1}{2} \cos(\vartheta) [\sqrt{n_0} + \sqrt{n_0 + 1}]^2 (N_{11}(0) + P_{11}(0)) \right]^2.$$

- ¹ A. F. Andreev and I. M. Lifshitz, Sov. Phys. JETP **29**, 1107 (1969).
- ² G. V. Chester, Phys. Rev. A **2**, 256 (1970).
- ³ A. J. Leggett, Phys. Rev. Lett. **25**, 1543 (1970).
- ⁴ E. Kim and M. H. W. Chan, Science **305**, 1941 (2004).
- ⁵ D. Jaksch, C. Bruder, J. I. Cirac, C. W. Gardiner, and P. Zoller, Phys. Rev. Lett. **81**, 3108 (1998), cond-mat/9805329.
- ⁶ M. P. A. Fisher, P. B. Weichman, G. Grinstein, and D. S. Fisher, Phys. Rev. B **40**, 546 (1989).
- ⁷ M. Greiner, O. Mandel, T. Esslinger, T. W. Hänsch, and I. Bloch, Nature **415**, 39 (2002).
- ⁸ D. vanOosten, P. vanderStraten, and H. T. C. Stoof, Phys. Rev. A **63**, 053601 (2001), cond-mat/0011108.
- ⁹ N. Elstner and H. Monien, Phys. Rev. B **59**, 012184 (1999), cond-mat/9807033.
- ¹⁰ G. G. Batrouni, R. T. Scalettar, and G. T. Zimanyi, Phys. Rev. Lett. **65**, 1765 (1990).
- ¹¹ S. Wessel, F. Alet, M. Troyer, and G. G. Batrouni, Phys. Rev. A **70**, 053615 (2004), cond-mat/0404552.
- ¹² N. Elstner and H. Monien, cond-mat/9905367 (1999).
- ¹³ S. R. Clark and D. Jaksch, New J. Phys. **8**, 160 (2006), cond-mat/0604625.
- ¹⁴ D. B. M. Dickerscheid, D. van Oosten, P. J. H. Denteneer, and H. T. C. Stoof, Phys. Rev. A **68**, 043623 (2003).
- ¹⁵ X. Lu, J. Li, and Y. Yu, Phys. Rev. A **73**, 043607 (2006), cond-mat/0504503.
- ¹⁶ K. Sengupta and N. Dupuis, Phys. Rev. A **71**, 033629 (2005), cond-mat/0412204.
- ¹⁷ Y. Ohashi, M. Kitaura, and H. Matsumoto, Phys. Rev. A **73**, 033617 (2006), cond-mat/0510725.
- ¹⁸ E. P. Gross, Nuovo Cimento **20**, 454 (1961).
- ¹⁹ L. P. Pitaevskii, Sov. Phys. JETP **13**, 451 (1961).
- ²⁰ A. A. Abrikosov, L. P. Gorkov, and I. E. Dzyaloshinski, *Methods of quantum field theory in statistical physics* (Dover, N.Y., 1963).
- ²¹ S. Sachdev, K. Sengupta, and S. M. Girvin, Phys. Rev. B **66**, 075128 (2002).
- ²² T. Stöferle, H. Moritz, C. Schori, M. Köhl, and T. Esslinger, Phys. Rev. Lett. **92**, 130403 (2004), cond-mat/0312440.
- ²³ C. Tozzo, M. Kramer, and F. Dalfovo, Phys. Rev. A **72**, 023613 (2005), cond-mat/0505625.
- ²⁴ C. Kollath, A. Iucci, T. Giamarchi, W. Hofstetter, and U. Schollwöck, Phys. Rev. Lett. **97**, 050402 (2006), cond-mat/0603721.
- ²⁵ A. Iucci, M. A. Cazalilla, A. F. Ho, and T. Giamarchi, Phys. Rev. A **73**, 041608(R) (2006), cond-mat/0508054.
- ²⁶ J. S. Caux and P. Calabrese, cond-mat/0603654 (2006).
- ²⁷ J. Stenger, S. Inouye, A. P. Chikkatur, D. M. Stamper-Kurn, D. E. Pritchard, and W. Ketterle, Phys. Rev. Lett. **82**, 4569 (1999), cond-mat/9901109.
- ²⁸ D. vanOosten, D. B. M. Dickerscheid, B. Farid, P. vanderStraten, and H. T. C. Stoof, Phys. Rev. A **71**, 021601(R) (2005), cond-mat/0405492.
- ²⁹ G. G. Batrouni, F. F. Assaad, R. T. Scalettar, and P. J. H. Denteneer, Phys. Rev. A **72**, 031601(R) (2005), cond-mat/0503371.
- ³⁰ A. Reischl, K. P. Schmidt, and G. S. Uhrig, Phys. Rev. A **72**, 063609 (2005), cond-mat/0504724.
- ³¹ E. Altman and A. Auerbach, Phys. Rev. Lett. **89**, 250404 (2002).
- ³² A. Auerbach, *Interacting Electrons and Quantum Magnetism* (Springer-Verlag New-York, 1994).
- ³³ J. Avery, *Creation and annihilation operators* (McGraw-Hill, 1974).
- ³⁴ S. Sachdev, *Quantum Phase Transitions* (Cambridge University Press, 1999).
- ³⁵ M. Greiner, O. Mandel, T. W. Hänsch, and I. Bloch, Nature **419**, 51 (2002).
- ³⁶ D. S. Rokhsar and B. G. Kotliar, Phys. Rev. B **44**, 10328 (1991).
- ³⁷ S. Defago, S. D. Huber, and G. Blatter (2006), to be published.
- ³⁸ The integral (32) is calculated numerically by determining lines of constant energy $\hbar\omega$ and integrating $P(\mathbf{q}, \mathbf{k})$ along these lines. The extension to three dimensions is straightforward and can be efficiently done via a determination of constant energy surfaces using Monte-Carlo sampling.
- ³⁹ S. D. Huber (2004), diploma thesis, unpublished.
- ⁴⁰ For an isotropic lattice modulation, the expansion of the constraint can be avoided as the operator T can be expressed as the difference between H and local terms.
- ⁴¹ M. Kramer, C. Tozzo, and F. Dalfovo, Phys. Rev. A **71**, 061602(R) (2005), cond-mat/0410122.
- ⁴² C. Schori, T. Stöferle, H. Moritz, M. Köhl, and T. Esslinger, Phys. Rev. Lett. **93**, 240402 (2004), cond-mat/0408449.
- ⁴³ The method of Dyson and Maleev,^{44,45} which is known to give better approximations for spin-waves in ferromagnets than the Holstein-Primakoff approach, is not applicable in our case due to the lack of the small parameter $1/S$, where S is the magnitude of the spin.
- ⁴⁴ F. J. Dyson, Phys. Rev. **102**, 1217 (1956).
- ⁴⁵ S. V. Maleev, Sov. Phys. JETP **6**, 776 (1958).
- ⁴⁶ R. Sooryakumar and M. V. Klein, Phys. Rev. Lett. **45**, 660 (1980).
- ⁴⁷ X. L. Lei, C. S. Ting, and J. L. Birman, Phys. Rev. B **32**, 1464 (1985).